

Influence of elevated radiative lifetime on efficiency of CdSe/CdTe Type II colloidal quantum dot based solar cells

Marina A. Leontiadou^a, Edward J. Tyrrell^b, Charles T. Smith^a,
Daniel Espinobarro-Velazquez^a, Robert Page^c, Paul O'Brien^c, Jacek Miloszewski^b,
Thomas Walsh^b, David Binks^a, Stanko Tomić^{b,*}

^a School of Physics and Astronomy & Photon Science Institute, University of Manchester, Manchester M13 9PL, United Kingdom

^b Joule Physics Laboratory, School of Computing, Science and Engineering, University of Salford, Manchester M5 4WT, United Kingdom

^c School of Chemistry, University of Manchester, Manchester M13 9PL, United Kingdom

ARTICLE INFO

Article history:

Received 11 July 2015

Received in revised form

11 December 2015

Accepted 17 January 2016

Keywords:

Efficiency

Solar cells

Colloidal quantum dots

Core/shell structure

ABSTRACT

Colloidal quantum dots (CQDs) are promising materials for solar cells because their optoelectronic properties are easily adjusted by control of their size, structure and composition. We present calculations of the band gap and radiative lifetime for varying core diameter and shell thickness of CdSe/CdTe core/shell Type II CQDs using a combination of single particle (2,6)-band $\mathbf{k} \cdot \mathbf{p}$ and many-electron configuration interaction (CI) Hamiltonians. These calculations are validated by comparison with experimental absorption spectra and photoluminescence decay data. The results are then incorporated into a model of photovoltaic efficiency which demonstrates how the overall performance of a solar cell based on Type II CQDs is affected by changes in the core/shell geometry. The largest effect on photovoltaic efficiency is found to be due to the longer radiative lifetime produced by increasing the shell thickness.

© 2016 Published by Elsevier B.V.

1. Introduction

Colloidal quantum dots (CQDs) are nanoscale crystals of semiconductor that are sufficiently small to confine charge carrier wave functions. This effect allows the effective band gap, E_g , of CQDs to be size-tuned which, coupled with the facile and inexpensive solution-based techniques by which they can be synthesised and processed, makes them promising photo-absorbing species for solar cells [1], as well as having other application in displays [2,3], lighting [3,4] and photorefractive devices [5]. The appeal of CQDs for solar energy conversion is further increased by the possibility of the efficient generation of more than one electron–hole pair per absorbed photon, by a process known either as multiple exciton generation or carrier multiplication [6]. Progress in CQD-based solar cells has been particularly rapid in recent years [1] with the development of effective surface passivation techniques using halide ions, resulting in enhanced efficiency with the record under unconcentrated sunlight currently standing at 9.9% [7].

Reducing the size of CQDs increases E_g relative to its bulk value. This means that size-tuning can be used to optimise the effective optical gap of CQDs for solar conversion if they are composed of a

material which has a bulk E_g that is too small for effective exploitation of the solar spectrum. Examples of such CQD materials include PbS and PbSe which have bulk band gaps of 0.41 eV [8] and 0.28 eV [9], respectively. The corollary of this is that size tuning cannot be used to reduce E_g towards the optimum value. However, a shell of a different semiconductor material can be grown around a CQD, and this so-called core/shell geometry allows the photo-physical properties to be controlled in a different way to size-tuning. For instance, for some combinations of core and shell material, the band offsets are such that a “Type II” heterojunction is formed, which causes electrons and holes to localise in different regions (in a Type I configuration, both charge carriers localise to the same region). The absorption edge of such a Type II core/shell CQD corresponds to a transition from the valence band maximum (VBM) of one of the materials to the conduction band minimum (CBM) of the other, and the energy of this transition may be less than the bulk band gap of either of the materials that comprise the CQD [10]. A Type II structure thus allows E_g to be reduced towards the optimum, but it will also affect photo-physical properties of CQDs in other ways that determine their efficacy as the photo-absorbing species in a solar cell. In particular, localisation of the electron and hole into different regions of the CQDs reduces the overlap of their wave functions. This will tend to increase the radiative recombination lifetime, τ_{rad} , and hence

* Corresponding author. Tel.: +44 161 295 3847.
E-mail address: s.tomic@salford.ac.uk (S. Tomić).

increase the probability that photo-generated charges will escape the CQD and be collected at the electrodes of the cell.

Optimisation of the design of a Type II CQD for application as the photo-absorbing species in a solar cell requires an understanding of how combinations of core diameter and shell thickness simultaneously affect the properties of CQDs important to photovoltaic performance. The properties of Type II CQDs have been calculated previously by a number of techniques including effective mass modelling [11,12] and a quantum Monte Carlo approach [13], with most of this work focusing on CQDs composed of the cadmium chalcogenide materials for which synthesis techniques are very well-developed. We have recently shown [14] that the most accurate description of Type II Cd-based CQDs requires the incorporation in the model of both configuration interactions and polarisation effects at the CQD surface.

In this work, we use this model to investigate how both E_g and τ_{rad} change with core diameter and shell thickness for CdSe/CdTe core/shell Type II CQDs. The results of these calculations are validated by comparison with experimental data, and are also incorporated into a model of photovoltaic efficiency that describes how the overall performance of a cell based on Type II CQDs is affected by changes in the core/shell geometry.

2. Methodology

2.1. Theory

In order to describe the electronic structure of CdSe/CdTe CQDs, we perform calculations using $\mathbf{k} \cdot \mathbf{p}$ theory in conjunction with the CI method. The (2,6)-band $\mathbf{k} \cdot \mathbf{p}$ Hamiltonian, $\hat{H}^{(\mu)}$, for spherically symmetric CQD heterostructures is used to calculate single-particle states in core/shell CQDs; this theory takes into account the complex band mixing, the spin-orbit interaction, and correct operator ordering at the core/shell and shell/colloid hetero-interfaces. The Schrödinger equation for the single-particle states can be written as follows:

$$\hat{H}^{(\mu)} \varphi_{njmp}^{(\mu)} = E_{njp}^{(\mu)} \varphi_{njmp}^{(\mu)} \quad (1)$$

where $\mu = \{e, h\}$ denote electron or hole single-particle states, $\varphi_{njmp}^{(\mu)}$ is the single-particle wave function, $E_{njp}^{(\mu)}$ is the single-particle energy, n is the principle quantum number, j is the total angular momentum, m is the z-component of the total angular momentum, and p is the eigenvalue of the parity operator. In the (2,6)-band $\mathbf{k} \cdot \mathbf{p}$ theory the electron (hole) wave function is given by:

$$\varphi_{njmp}^e(\mathbf{r}) = \sum_{J_z = -1/2}^{1/2} F_{1/2J_z}^{e,njmp}(\mathbf{r}) u_{1/2J_z}^e \quad (2)$$

and

$$\varphi_{njmp}^h(\mathbf{r}) = \sum_{J_z = 1/2}^{3/2} \sum_{J_z} F_{JJ_z}^{h,njmp}(\mathbf{r}) u_{JJ_z}^h \quad (3)$$

where $u_{JJ_z}^\mu$ represents the Bloch function of the conduction (valence) band, J and J_z are the Bloch function angular momentum and its z-component, respectively, and $F_{JJ_z}^{\mu,njmp}(\mathbf{r})$ are envelope functions which contain the angular and radial dependences of the wave functions; full definitions are given in Refs. [11,14,15]. Due to the spherical symmetry of the system, the eigen-energies are $(2j+1)$ -fold degenerate with respect to the quantum number m . The eigen-energies of single-particle levels are calculated by numerically solving the equations resulting from imposing continuity of the radial wave functions and radial component of the probability current across the heterointerfaces [15]. The material parameters used to calculate single-particle states are listed in Ref. [14].

We denote single-particle states using the spectroscopic notation $n l_j^{(\mu)}$ where $l = s, p, d, \dots$ represents the lowest value of the orbital angular momentum in the wave function. The eigenvalue p of the parity operator takes the values 1 and -1 for even and odd symmetry states, respectively. The dielectric constant varies significantly between the CQD and the surrounding colloidal material. Such variation produces very strong dielectric confinement and its effect on the excitonic structure cannot be neglected. In the presence of a spatially varying dielectric constant, the exciton Hamiltonian may be written as:

$$\hat{H}_X = \hat{H}^e + \hat{H}^h + V_c(\mathbf{r}_e, \mathbf{r}_h) + V_s(\mathbf{r}_e) + V_s(\mathbf{r}_h) \quad (4)$$

where V_c is the interparticle Coulomb potential and V_s is the self-polarisation potential due to the interaction of a carrier with its own polarisation charge. In contrast to epitaxial QDs [16], the large dielectric mismatch between CQDs and the surrounding solvent necessitates the inclusion of self-polarisation terms in the Hamiltonian. We note that $V_c = V_p + V_d$ where V_d is the direct inter-particle Coulomb potential and V_p is the interface polarisation potential [11]. We calculate the potentials V_c and V_s using the numerical model of Bolcatto and Proetto for finite size dielectric interfaces [17].

Correlated exciton states are solutions of the Schrödinger equation

$$\hat{H}_X \Psi_X^{L,L_z} = E_X \Psi_X^{L,L_z} \quad (5)$$

where L is the total exciton angular momentum, L_z is its z-component and E_X is the exciton eigen-energy. To construct excitonic states, we couple single particle states in terms of angular momentum rather than parity. Using the solutions of Eq. (1), $\varphi_{njmp}^{(\mu)} = |njmp\rangle$, we define the new ket notation, $|njmp\rangle$, expressed in terms of both total angular momentum j and the lowest value of orbital angular momentum l . In such notation the transformation between l, j and p is given as $l = j - p/2$ for electrons and $l = \min(j + p/2, |j - 3p/2|)$ for holes, where $p = +1(-1)$ for even (odd) states regardless of whether electron or hole states are considered [15]. We expand the exciton wave function in terms of uncorrelated electron-hole pair (EHP) states as:

$$\Psi_X^{L,L_z} = \sum_{\beta} c_{\beta} |n_e l_e j_e m_e n_h l_h j_h m_h; L, L_z\rangle \quad (6)$$

where

$$|n_e l_e j_e m_e n_h l_h j_h m_h; L, L_z\rangle = \sum_{m_e, m_h} C_{j_e m_e j_h m_h}^{L, L_z} |n_e l_e j_e m_e\rangle |n_h l_h j_h m_h\rangle \quad (7)$$

and $C_{j_e m_e j_h m_h}^{L, L_z}$ and c_{β} represent a Clebsch-Gordan coefficient and the expansion coefficients (character) of a particular EHP state labelled by β , respectively. The exciton Hamiltonian is then diagonalised in the basis of EHPs to find the exciton energies and wave functions; this is sometimes called direct diagonalisation or the configuration interaction (CI) method [16].

2.2. CQD synthesis

The CQDs were synthesised via the hot injection method using dual precursors. The CdSe cores were grown with a zinc-blende crystal structure following the method reported in Ref. [18], while the CdTe shell was grown by the dropwise method previously reported in Ref. [19]. After completion of the shelling process the CQDs were cooled at room temperature and stored under nitrogen.

2.3. Optical characterisation techniques

For optical characterisation the samples were placed in 10 mm path length quartz cuvettes (Starna) and diluted with toluene. The steady state absorption and the PL spectra were measured with

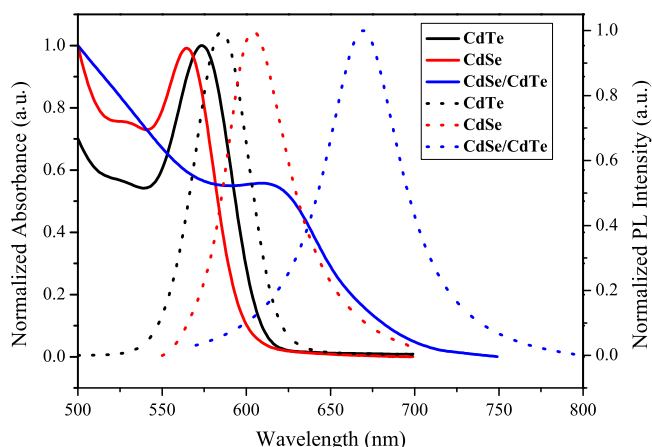


Fig. 1. Absorption (full lines) and PL (dashed lines) spectra for typical CdSe (red) and CdTe (black) core only QDs and CdSe/CdTe core/shell QDs (blue). The core radius was 1.6 nm for the CdTe QDs and 1.7 nm for both the CdSe core only and the core/shell QDs; the CdTe shell thickness was 0.9 nm. (For interpretation of the references to colour in this figure caption, the reader is referred to the web version of this paper.)

the use of a Perkin Elmer Lambda 1050 UV/Vis/NIR spectrometer and a Horiba Jobin Yvon Fluorolog model iHR(FL3-22) spectrofluorometer, respectively. The PL excitation wavelength was 450 nm with a bandwidth of 3 nm. Typical absorbance and PL spectra for CdSe, CdTe, and CdSe/CdTe QDs are shown in Fig. 1.

The PL time decay measurements were recorded using a time correlated single photon counting (TCSPC) system. A mode-locked Ti:sapphire laser (Mai Tai HP, Spectra-Physics) was used to generate 100 fs pulses at 80 MHz repetition rate and 820 nm wavelength. The repetition rate was reduced to 2 MHz by an acousto-optic pulse picker (APE Pulse Select), and the initial output was converted to 410 nm via second harmonic generation (APE HarmoniXX). These pulses were used to excite the sample with an average excitation power of 2.5 mW, with a spot size of 2.8 mm and hence a fluence of approximately 20 nJ/cm². The PL emission of the sample was directed into a monochromator (Spex 1870c) and detected by a multi-channel plate (Hamamatsu R3809U-50). The TCSPC electronics were from Edinburgh Instruments.

3. Results and discussions

3.1. Absorption edge wavelength of CdSe/CdTe Type II QDs

We proceed our analysis with the examination of the influence of CdSe/CdTe core/shell CQD morphology on the variation of the first exciton peak in the absorption spectra, which corresponds to excitation of the $1S_{1/2}^e 1S_{3/2}^h$ state. As a first step, we validate our theoretical methodology, Section 2.1, based on the combination of (2,6)-band $\mathbf{k} \cdot \mathbf{p}$ and CI Hamiltonians, against available experimental and theoretical results on CdSe and CdTe core only CQD, as they are the constituent materials of our core/shell structure. Fig. 2 shows variation of the $1S_{1/2}^e 1S_{3/2}^h$ exciton energy as a function of CdSe and CdTe QD radius, a_c , respectively. Solid symbols represent experimental results from several independent measurements from different groups and the line is an empirical inverse polynomial fitting curve, $E_X^{1S_{1/2}^e 1S_{3/2}^h}(a_c) = E_g^{\text{bulk}} + (Aa_c^2 + Ba_c + C)^{-1}$, to this experimental data proposed by de Mello Donega in Ref. [20], where A , B , and C are fitting parameters. Results of $1S_{1/2}^e 1S_{3/2}^h$ exciton energies predicted by our calculation are shown on the same figures and exhibit excellent agreement with the experimental measurements [21–30]. Such agreement confirms the accuracy of our methodology and parameter set for the lowest

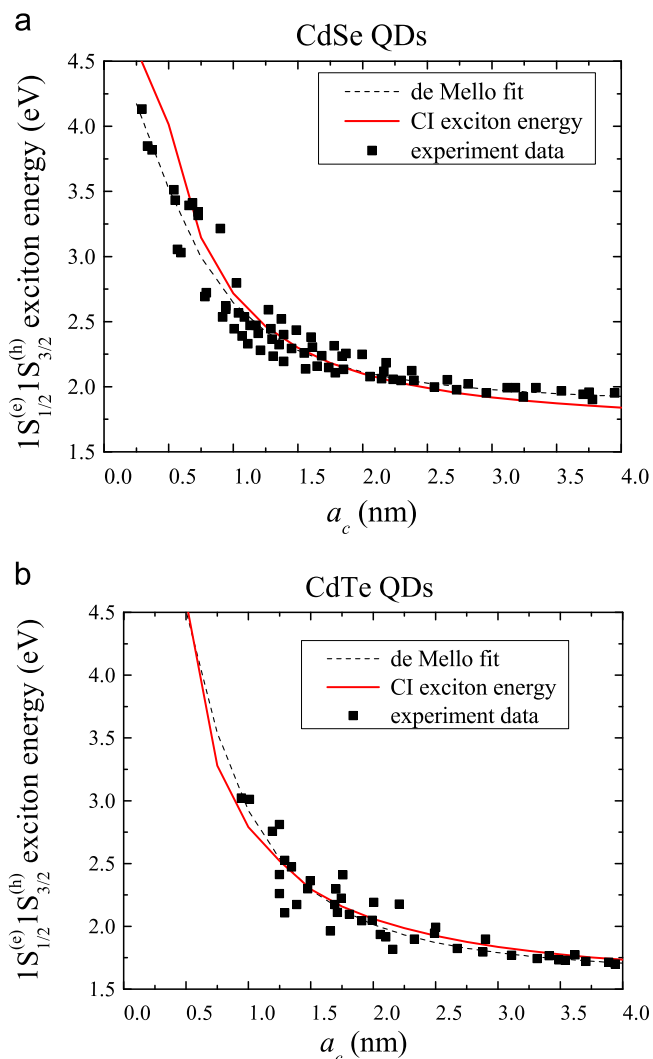


Fig. 2. Variation of the $1S_{1/2}^e 1S_{3/2}^h$ exciton energy as a function of CQD core radius, a_c , in (a) CdSe and (b) CdTe QDs: experimental results (black square symbols), de Mello Donega's empirical fit to the experimental data (dotted line) [20], and results of our (2,6)-band $\mathbf{k} \cdot \mathbf{p}$ and CI model (solid line).

excitonic state in both CdSe and CdTe QDs over a wide range of CQD sizes.

Having been validated for core-only CQD structures, we now employ our method to describe CdSe/CdTe core/shell Type II CQD structures. The remaining question when modelling the system of core/shell structures is the parametrisation of the valence band offset (VBO) between core and shell materials, in our case CdSe and CdTe, respectively. From our previous analysis [14] of the variation of $1S_{1/2}^e 1S_{3/2}^h$ and $1S_{1/2}^e 2S_{3/2}^h$ excitonic energies with the shell thickness in CdTe/CdSe core/shell CQD, we have estimated the $\text{VBO}_{\text{CdTe/CdSe}} = 0.4$ eV. We have assumed the same VBO for inverse structures, i.e., for CdSe/CdTe core/shell CQD considered here.

In contrast to core-only CQDs, the size dependence of $1S_{1/2}^e 1S_{3/2}^h$ exciton energies in core/shell CQDs is more complex and it is not possible to capture its trend by simple polynomial fitting curve. Fig. 3 shows the shell thickness, a_s , dependence of the $1S_{1/2}^e 1S_{3/2}^h$ absorption wavelengths for CdSe/CdTe core/shell CQDs for different core radii, a_c , ranging from $a_c = 1.5$ nm to 2.5 nm.

Also shown in Fig. 3 are experimental data for a CdSe core of 1.7 nm radius, as measured by transmission electron microscopy, and different CdTe shell thicknesses [31,45]. Good agreement is seen between the calculated energy of the $1S_{1/2}^e 1S_{3/2}^h$ exciton and

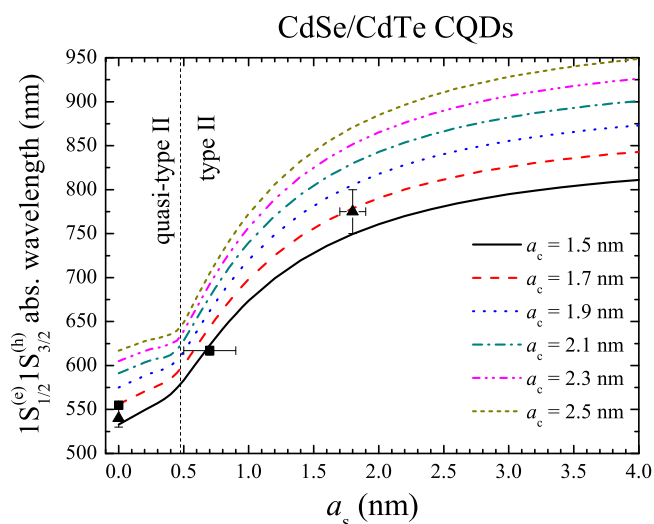


Fig. 3. Core radius, a_c , and shell thickness, a_s , dependence of the $1S_{1/2}^e 1S_{3/2}^h$ exciton peak in the absorption spectra of CdSe/CdTe core/shell QDs. Also shown for comparison are experimental data from Ref. [31] (squares) and Ref. [45] (triangles).

the spectral position observed for the first absorption peak, further validating our theoretical approach.

We can clearly distinguish between two trends in the $1S_{1/2}^e 1S_{3/2}^h$ absorption wavelengths in the region of shell thicknesses < 0.5 nm and for shell thicknesses > 0.5 nm. For the QDs with shells of thickness approximately or less than 0.5 nm, we can see that (i) the $1S_{1/2}^e 1S_{3/2}^h$ absorption wavelengths are approximately linearly dependent on a_s , suggesting strong influence of the dielectric confinement on $1S_{1/2}^e 1S_{3/2}^h$ excitons and their wavelengths in this region and (ii) as the core size, a_c , increases the gradient of the $1S_{1/2}^e 1S_{3/2}^h$ absorption wavelength vs. a_s curves decreases. We explain such non-monotonic behaviour in terms of the changing localisation regime of the $1S_{3/2}^h$ single-particle hole, in the correlated $1S_{1/2}^e 1S_{3/2}^h$ exciton, as the QD dimensions change [14]. The lower gradient of the curves for shell widths < 0.5 nm is due to the fact that the $1S_{3/2}^h$ hole is in the delocalised regime, i.e., its probability density is spread over the whole heterostructure and its energy is mainly determined by the global confinement provided by the QD potential well of radius $a_c + a_s$. In this regime the size dependence of the hole confinement is closer to that of one confined in a core-only QD. For the QDs with shells of width greater than 0.5 nm, we can see that the $1S_{1/2}^e 1S_{3/2}^h$ absorption wavelengths again acquire a trend that can be described by a quadratic polynomial function. As a_s increases, for a particular core size, the $1S_{3/2}^h$ single-particle hole localises in the shell fully so the absorption wavelength is again more strongly affected by the effect of shell thickness on the confinement energy of $1S_{3/2}^h$. This behaviour is closer to the strong confinement regime in a core/shell heterostructure. Maps of the absorption wavelength against QD core/shell dimensions, as depicted in Fig. 3, can only be obtained numerically and should be of use to experimentalists studying such systems.

3.2. Radiative lifetimes in CdSe/CdTe QDs

In order to assess the variation of the radiative times, τ_{rad} , with the core sizes, a_c , and shell thicknesses, a_s , we use the following expression:

$$\frac{1}{\tau_{\text{rad}}} = \frac{d_X}{3} \frac{F^2 \bar{n} e^2}{\pi \epsilon_0 m_0 c^3 \hbar^2} E_X E_P |\mathbf{P}_X|^2 \quad (8)$$

where \bar{n} is the refractive index of the colloidal material, e is the electron charge, ϵ_0 is the permittivity of free space, m_0 is the

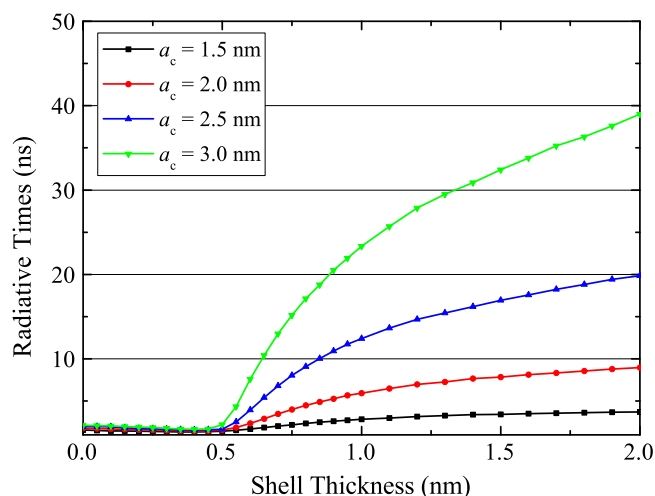


Fig. 4. Plot of radiative lifetime against shell thicknesses $a_c = 1.5, 2.0, 2.5$ and 3.0 nm CdSe/CdTe QDs, calculated using the CI method.

electron rest mass, c is the speed of light, \hbar is the reduced Planck constant, and $E_P = 2P^2/m_0$, where P is the optical dipole matrix element of the bulk material at the Γ point. In the expression above $|\mathbf{P}_X|$ is the modulus of excitonic dipole matrix element and E_X is the excitonic energy, obtained both from the CI calculation, and d_X is the integer number representing the degree of degeneracy of a particular excitonic state. For the $1S_{1/2}^e 1S_{3/2}^h$ exciton considered below $d_X = 8$. The expression for dielectric screening of spherical core/shell QDs is given as $F = 3\epsilon_{\text{coll}} / (2\epsilon_{\text{coll}} + \epsilon_{\text{QD}})$, where ϵ_{QD} is the dielectric constants the dot and ϵ_{coll} is the dielectric constant of the surrounding medium.

Fig. 4 shows the mean radiative lifetime of the $1S_{1/2}^e 1S_{3/2}^h$ exciton in CdSe/CdTe QDs as a function of shell thickness a_s for several different core radii. The most noticeable feature is the sudden increase in τ_{rad} at around $a_s \sim 0.5$ nm. In comparison to core-only QDs, in which the value of $1S_{1/2}^e 1S_{3/2}^h$ excitonic radiative time, τ_{rad} , changes relatively weakly with the QD size [32,33], in core/shell structures it is possible to increase this radiative time over one order of magnitude with suitable change in the core and shell sizes. Several observations regarding the trend in τ_{rad} in CdSe/CdTe core/shell Type II QDs can be made here: (i) again as in the case of the absorption wavelength, shown in Fig. 3, we can distinguish clearly between two different regions of the shell thicknesses $a_s < 0.5$ nm and $a_s > 0.5$ nm. In the region of $a_s < 0.5$ nm the whole QD system behaves similar to core-only QDs, since both electron and hole correlated charge densities are either largely confined in the core region or just start to delocalise over the whole QD structure. In this region the optical dipole matrix element, $|\mathbf{P}_X|$, is strong while the magnitude of both $|\mathbf{P}_X|$ and E_X changes very little with the overall sizes of QDs, which explains the almost constant τ_{rad} . (ii) As shell thicknesses increase, and in particular beyond $a_s > 1$ nm, the hole states become strongly confined in the shell region. Here dielectric confinement does not have enough strength to overcome the confinement imposed by the Type II aligned valence band edge of CdTe, so that the exciton reaches the strong confinement regime. Consequently, the electron-hole wave function overlap is dramatically reduced, and E_X is mainly now determined by the variation of the $1S_{3/2}^h$ hole confinement with a_s . For $a_s > 1$ nm, τ_{rad} continues to increase, but more slowly, reaching values that are about one order of magnitude greater than those for core-only QDs. For all shell thicknesses, a monotonic trend to larger τ_{rad} with increasing core size is also observed. It is interesting to observe that for CdSe/CdTe Type II QDs the value of τ_{rad} increases over “only” one order of magnitude while in other systems, such as epitaxially grown Type

II InAs/GaAs/GaAsSb, a Type II structure the radiative times can increase over three order of magnitudes [34,35]. This difference in behaviour is attributed to the absence of significant dielectric confinement in epitaxially grown QDs, compared to CQDs.

The interplay between the excitonic energy, radiative times and absorption characteristics is intimately connected by the magnitude of the excitonic optical dipole. In the Type-II configuration, as we have shown previously [36,37], the electron and hole are spatially separated, that is the wavefunction overlap becomes smaller when compared with the equivalent Type I structure. However, our previous analysis [36] suggests that the reduction of the absorption strength due to Type II alignment compared to the Type-I configuration is evident at the absorption edge while overall absorption characteristics are similar. However this change in absorption characteristics may reduce the overall efficiency of CQD solar cells, and will be discussed elsewhere.

As for the calculations of the band gap described above, we also validate the values of radiative lifetime produced by our model by comparing them to experimental data. Fig. 5 shows example experimental PL decay transients for CdSe core-only CQDs, and for CdSe/CdTe CQDs comprising the same core and two different CdTe shell thicknesses. The first absorption peak for these CQDs, which corresponds to the $1S_{1/2}^e 1S_{3/2}^h$ exciton, was observed at 555 nm, 630 nm and 713 nm. Using the data presented in Figs. 2 and 3, these wavelengths indicate that the core radius is 1.6 nm and the shell thicknesses in the two CdSe/CdTe CQD samples are 1 nm and 2 nm, respectively. In each case, the PL decay transient is not mono-exponential in form, indicating that recombination dynamics are significantly affected by surface trapping [33,38,39]. The transients are well-described by a tri-exponential decay function $y(t) = A_{\text{rad.}} \exp(-t/\tau_{\text{rad.}}) + A_1 \exp(-t/\tau_1) + A_2 \exp(-t/\tau_2)$ where t is the time and $A_{\text{rad.}}$, A_1 , A_2 , τ_1 and τ_2 are the fitting parameters while the $\tau_{\text{rad.}}$ is the radiative time. Similar behaviour

has been reported previously for CdSe [40–42], CdTe [33,40], CdTe/CdSe [40] and CdSe/ZnS CQDs [43]. The tri-exponential form of the decay has been explained by Gong et al. [40] with a model that includes capture and escape from a shallow trap state related to an under-coordinated surface atom. Recent calculations [44] based on an Auger-mediated trapping model have identified under-coordinated Te atoms on the surface of CQDs as the source of hole-traps at an energy just 50 meV above the VBM, from which thermally excited escape is thus possible. In this model, one of the three time constants can be identified directly with $\tau_{\text{rad.}}$, assuming that the fraction of CQDs that do not emit at all are primarily responsible for the quantum yield being less than unity [40]. We therefore fixed one of the time constants of a tri-exponential decay function to be equal to the calculated value $\tau_{\text{rad.}}$ and fitted it to the experimental PL decay data, with all other fitting parameters free to vary. As shown in Fig. 5, this procedure resulted in excellent agreement between the data and the fit, demonstrating that the values of $\tau_{\text{rad.}}$ calculated are consistent with experiment.

The parameter values resulting from this fitting process are given in Table 1. In comparison, for a 1.7 nm radius CdSe core Chen et al. [45] also report a non-monoexponential PL decay transient, to which they fit a biexponential function. The major component of this fit has a lifetime of 18 ns, which is comparable to the value of τ_1 given in Table 1 for the CdSe core only CQD. Chen also reports that the lifetime corresponding to this major component increases to 29 ns on the addition of a 1.8 ± 0.1 nm thick CdTe shell, which is bounded by the values of τ_1 for shells of 1.0 ± 0.2 nm and 2 ± 0.2 nm thickness given in Table 1. The results described by Chen et al. [45] for a similar CdSe/CdTe CQD are thus consistent with the ones observed for our samples.

3.3. Solar cell efficiency

A limit for the theoretical maximum efficiency of a conventional solar cell can be calculated using the “detailed balance” model [46], where whilst in thermal equilibrium under solar illumination, four unavoidable losses [47,48] are considered: (1) photons with energy below E_g are not absorbed; (2) carrier energy in excess of the bandgap is lost as heat; (3) thermodynamic loss—the available energy (Gibbs free energy or chemical potential) of the thermalised excited states is always less than the internal energy, with the consequence that the photovoltage (or, output chemical potential) must be less than E_g ; and (4) radiative recombination: a small fraction of the excited states radiatively recombine with the ground states at maximum power output.

The wavelength-dependent flux of solar radiation is integrated such that all photons with energy above E_g produce a single exciton at the band edge, producing a photo-generated current density given by $I_{\text{pg}} = e \int_{E_g}^{\infty} \phi(h\nu) d(h\nu)$ where $\phi(h\nu)$ is the spectral photon flux density. This is offset by a loss of photogenerated current due to recombination, given by modelling black body radiation of the solar cell at room temperature: $I_r = (2\pi e/h^3 c^2) \int_{E_g}^{\infty} \{(h\nu)^2 / \exp[(h\nu - eV)/k_B T] - 1\} d(h\nu)$, where h is Planck's constant, k_B is Boltzmann's constant, T is the temperature (set to 300 K here) and V is the operating voltage of the cell. V is assumed to be equal to a constant quasi-Fermi level separation and is numerically optimised to give the maximum efficiency, which is

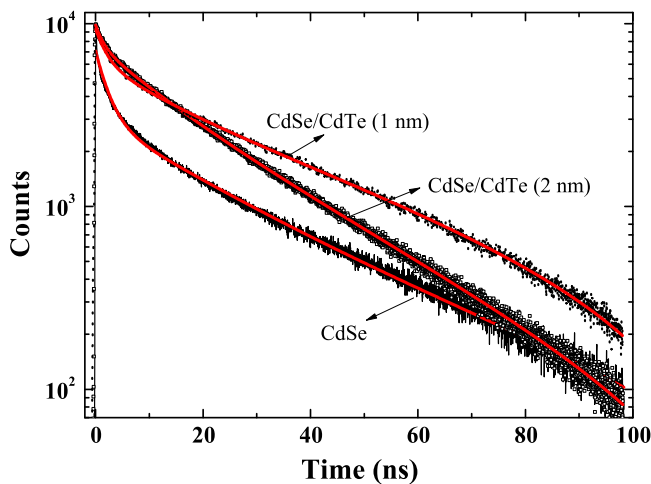


Fig. 5. Experimental photoluminescence decay transients (black) for CdSe core-only CQDs with $a_c = 1.6$ nm, and CdSe/CdTe CQDs made from the same cores and with shell thickness of 1 nm and 2 nm. Also shown are tri-exponential fits (red) to the data for which one of the time constants has been set to the calculated value of $\tau_{\text{rad.}}$ for that core size and shell thickness. (For interpretation of the references to colour in this figure caption, the reader is referred to the web version of this paper.)

Table 1

Parameters yielded from the fits shown in Fig. 5. $\tau_{\text{rad.}}$ (ns) are fixed to calculated values.

Sample (a_s)	$A_{\text{rad.}}$	$\tau_{\text{rad.}}$ (ns)	A_1	τ_1 (ns)	A_2	τ_2 (ns)
CdSe (0 nm)	3154 ± 18	2.3	3076 ± 50	23.7 ± 0.1	3202 ± 29	0.25 ± 0.01
CdSe/CdTe (1 nm)	3214 ± 53	11.7	4548 ± 39	28.0 ± 0.2	2101 ± 15	1.44 ± 0.02
CdSe/CdTe (2 nm)	1993 ± 44	11.1	4665 ± 17	45.2 ± 0.5	3006 ± 18	1.97 ± 0.02

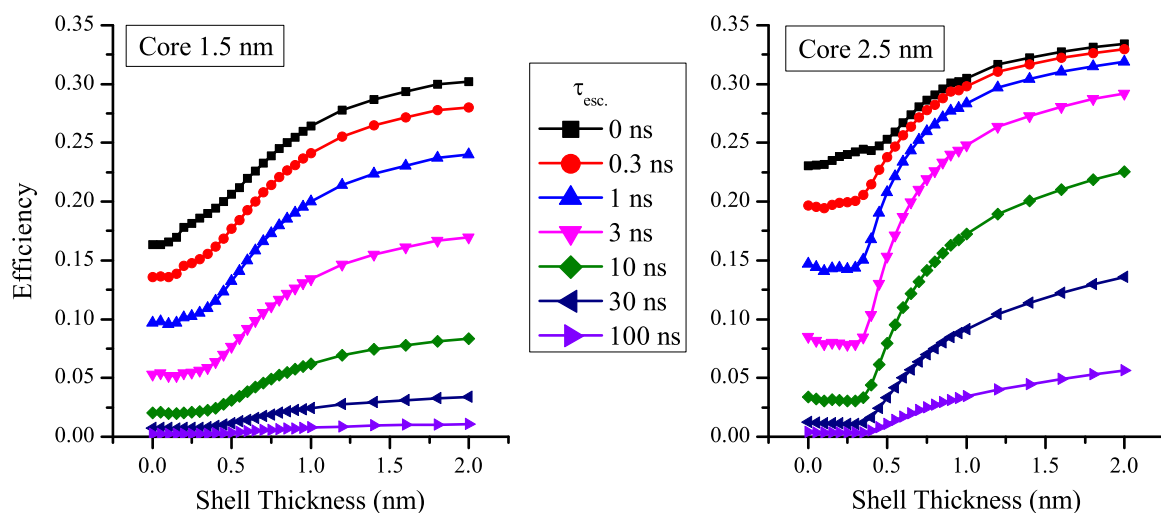


Fig. 6. Solar cell efficiency given by the modified detailed balance model for cells sensitised with CdSe/CdTe Type II CQD for core radii of 1.5 nm (left) and 2.5 nm (right) and varying shell thicknesses and lifetime of charge carrier escape, τ_{esc} .

the ratio of output power to input power, given by $\eta_{\text{pv}} = (I_{\text{pg}} - I_{\text{r}}) \cdot V / E_e$, where E_e is the total solar irradiance. Here the total irradiance and solar flux are set to the AM1.5G solar spectrum [49]. Full details of the model can be found elsewhere [50].

We consider a fifth loss in the system which utilises the probability, P_{esc} , of a cooled exciton escaping from a CQD and contributing to the photocurrent before radiative recombination occurs. This can be expressed in terms of the characteristic lifetime of the escape process, τ_{esc} , and the radiative lifetime, τ_{rad} , as

$$P_{\text{esc}} = \frac{\tau_{\text{esc}}^{-1}}{\tau_{\text{rad}}^{-1} + \tau_{\text{esc}}^{-1}} \quad (9)$$

For core sizes of 1.5 nm and 2 nm the efficiencies predicted by this model for solar cells utilizing CdSe/CdTe CQDs as the absorbing species are given in Fig. 6 with shell thicknesses up to 2 nm and τ_{esc} varying from 0.3 ns, indicating fast charge transfer as reported by some authors [51–53], to 100 ns. Also shown is the thermodynamic efficiency limit where $\tau_{\text{esc}} = 0$ and all charges escape the CQD. The optical band gaps used for these core sizes were those given in Fig. 3, and the radiative lifetimes for a given shell thickness in Fig. 4. The predicted efficiency of the device increases significantly with the thickness of the CdTe shell for both core sizes, primarily attributable to the change in radiative lifetime. As expected a long carrier escape lifetime can significantly reduce this efficiency, and so will be a crucial element to the effectiveness of any devices hoping to utilise thick shells, and poses a particular challenge to the preparation and environment of the CQDs. Effective passivation methods such as bulky ligands, surface treatment or additional shells which can dramatically increase the quantum yield of CQDs [39,54,55] have been shown to sometimes hinder charge extraction [51], and dramatically reduce the yield of photovoltaic devices where carriers are Coulombically bound to the CQD–surface molecule interface unless operated with an external field [56,57].

4. Conclusions

Using a combination of $\mathbf{k} \cdot \mathbf{p}$ theory and the CI method, the change in optical gap of CdSe/CdTe core/shell Type II CQDs has been predicted for varying core diameter and shell thickness. We have shown that the rate of change varies significantly as the hole states become strongly confined in the shell region, which was shown to occur when the shell thickness begins to exceed 1 nm.

This localisation primarily improves cell performance by the reduction in electron–hole wavefunction overlap and consequent increase in radiative lifetime it produces, but also provides a method of reducing the effective absorption edge energy which can be of benefit for wider band gap materials. This numerical method has been used to produce maps of absorption wavelength as a function of CQD geometry which cannot be well described by a simple inverse quadratic polynomial fit, as is often done for Type I systems [20,21,58]. This method was also used to calculate radiative lifetimes for the varying CQD geometries, for which a more dramatic variation is observed. For $a_s > 1$ nm, τ_{rad} reaches values of ~ 10 –40 ns, which is about one order of magnitude higher than that for thin or no shell at ~ 3 ns. These observations are validated by comparison with experimental photoluminescence decay curves, where the longest decay component shows strong agreement with the calculated τ_{rad} . The effect of increasing the shell thickness on solar cell performance was examined using a modified detailed balance model [46], in which the photovoltaic efficiency depends on both the band gap and the radiative lifetime. A significant increase in the potential device efficiency is predicted for the addition of shells greater than 1 nm in thickness principally due to the order of magnitude increase in radiative lifetime.

Acknowledgements

The authors acknowledge the EPSRC UK Grant “Enhanced multiple exciton generation in colloidal quantum dots” (EP/K008587/1) for financial support. We also acknowledge the EU-COST project “MultiscaleSolar” (MP1406) and the Royal Society Grant (RG120558) “High Performance Computing in Modelling of Innovative Photo-Voltaic Devices”. We acknowledge help from the N8 Research Partnership and Science and Technology Facilities Council for providing the computational resources used to conduct this research. We would also like to express our gratitude to W. Flavell for useful discussions.

References

- [1] G.H. Carey, A.L. Abdelhady, Z. Ning, S.M. Thon, O.M. Bakr, E.H. Sargent, Colloidal quantum dot solar cells, *Chem. Rev.* 115 (23) (2015) 12732–12763.
- [2] T.-H. Kim, K.-S. Cho, E.K. Lee, S.J. Lee, J. Chae, J.W. Kim, D.H. Kim, J.-Y. Kwon, G. Amarutunga, S.Y. Lee, B.L. Choi, Y. Kuk, J.M. Kim, K. Kim, Full-colour

- quantum dot displays fabricated by transfer printing, *Nat. Photonics* 5 (3) (2011) 176–182.
- [3] Y. Shirasaki, G.J. Supran, M.G. Bawendi, V. Bulovic, Emergence of colloidal quantum-dot light-emitting technologies, *Nat. Photonics* 7 (1) (2013) 13–23.
 - [4] S. Reineke, Complementary LED technologies, *Nat. Mater.* 14 (5) (2015) 459–462.
 - [5] F. Aslam, J. Stevenson-Hill, D. Binks, S. Daniels, N. Pickett, P. O'Brien, Effect of nanoparticle composition on the performance of photorefractive polymers, *Chem. Phys.* 334 (1–3) (2007) 45–52.
 - [6] C. Smith, D. Binks, Multiple exciton generation in colloidal nanocrystals, *Nanomaterials* 4 (1) (2013) 19.
 - [7] C.-H.M. Chuang, P.R. Brown, V. Bulović, M.G. Bawendi, Improved performance and stability in quantum dot solar cells through band alignment engineering, *Nat. Mater.* 13 (8) (2014) 796–801.
 - [8] M.N. Nordin, J. Li, S.K. Clowes, R.J. Curry, Temperature dependent optical properties of PbS nanocrystals, *Nanotechnology* 23 (27) (2012) 275701.
 - [9] R. Koole, G. Allan, C. Delerue, A. Meijerink, D. Vanmaekelbergh, A. Houtepen, Optical investigation of quantum confinement in PbSe nanocrystals at different points in the Brillouin zone, *Small* 4 (1) (2008) 127–133.
 - [10] U. Aeberhard, R. Vaxenburg, E. Lifshitz, S. Tomić, Fluorescence of colloidal PbSe/PbS QDs in NIR luminescent solar concentrators, *Phys. Chem. Chem. Phys.* 14 (2012) 16223–16228.
 - [11] E.J. Tyrrell, J.M. Smith, Effective mass modeling of excitons in type-II quantum dot heterostructures, *Phys. Rev. B* 84 (2011) 165328.
 - [12] A. Piryatinski, S.A. Ivanov, S. Tretiak, V.I. Klimov, Effect of quantum and dielectric confinement on the exciton-exciton interaction energy in type II core/shell semiconductor nanocrystals, *Nano Lett.* 7 (1) (2007) 108–115.
 - [13] P.G. McDonald, E.J. Tyrrell, J. Shumway, J.M. Smith, I. Galbraith, Tuning biexciton binding and antibinding in core/shell quantum dots, *Phys. Rev. B* 86 (2012) 125310.
 - [14] E.J. Tyrrell, S. Tomić, Effect of correlation and dielectric confinement on $1s_{1/2}^{(e)}$ $ns_{3/2}^{(h)}$ excitons in CdTe/CdSe and CdSe/CdTe type-II quantum dots, *J. Phys. Chem. C* 119 (22) (2015) 12720–12730.
 - [15] E.P. Pokatilov, V.A. Fonoberov, V.M. Fomin, J.T. Devreese, Development of an eight-band theory for quantum dot heterostructures, *Phys. Rev. B* 64 (2001) 245328.
 - [16] N. Vukmirovic, S. Tomić, Plane wave methodology for single quantum dot electronic structure calculations, *J. Appl. Phys.* 103 (10) (2008) 103718.
 - [17] P.G. Bolcatto, C.R. Proetto, Partially confined excitons in semiconductor nanocrystals with a finite size dielectric interface, *J. Phys.: Condens. Matter* 13 (2) (2001) 319.
 - [18] M.B. Mohamed, D. Tonti, A. Al-Salman, A. Chemseddine, M. Chergui, Synthesis of high quality zinc blende CdSe nanocrystals, *J. Phys. Chem. B* 109 (21) (2005) 10533–10537.
 - [19] N. McElroy, R. Page, D. Espinbarro-Valazquez, E. Lewis, S. Haigh, P. O'Brien, D. Binks, Comparison of solar cells sensitised by CdTe/CdSe and CdSe/CdTe core/shell colloidal quantum dots with and without a CdS outer layer, *Thin Solid Films* 560 (2014) 65–70.
 - [20] C. de Mello Donegá, R. Koole, Size dependence of the spontaneous emission rate and absorption cross section of CdSe and CdTe quantum dots, *J. Phys. Chem. C* 113 (16) (2009) 6511–6520.
 - [21] W.W. Yu, L. Qu, W. Guo, X. Peng, Experimental determination of the extinction coefficient of CdTe, CdSe, and CdS nanocrystals, *Chem. Mater.* 15 (14) (2003) 2854–2860.
 - [22] T. Rajh, O.I. Micic, A.J. Nozik, Synthesis and characterization of surface-modified colloidal cadmium telluride quantum dots, *J. Phys. Chem.* 97 (46) (1993) 11999–12003.
 - [23] C.B. Murray, D.J. Norris, M.G. Bawendi, Synthesis and characterization of nearly monodisperse CdE (E = sulfur, selenium, tellurium) semiconductor nanocrystallites, *J. Am. Chem. Soc.* 115 (19) (1993) 8706–8715.
 - [24] X. Peng, J. Wickham, A.P. Alivisatos, Kinetics of II–VI and III–V colloidal semiconductor nanocrystal growth: “focusing” of size distributions, *J. Am. Chem. Soc.* 120 (21) (1998) 5343–5344.
 - [25] A.L. Rogach, A. Kornowski, M. Gao, A. Eychmüller, H. Weller, Synthesis and characterization of a size series of extremely small thiol-stabilized CdSe nanocrystals, *J. Phys. Chem. B* 103 (16) (1999) 3065–3069.
 - [26] V.N. Soloviev, A. Eichhofer, D. Fenske, U. Banin, Molecular limit of a bulk semiconductor: size dependence of the “band gap” in CdSe cluster molecules, *J. Am. Chem. Soc.* 122 (11) (2000) 2673–2674.
 - [27] F.V. Mikulec, M. Kuno, M. Bennati, D.A. Hall, R.G. Griffin, M.G. Bawendi, Organometallic synthesis and spectroscopic characterization of manganese-doped CdSe nanocrystals, *J. Am. Chem. Soc.* 122 (11) (2000) 2532–2540.
 - [28] Y. Masumoto, K. Sonobe, Size-dependent energy levels of CdTe quantum dots, *Phys. Rev. B* 56 (1997) 9734–9737.
 - [29] D.V. Talapin, S. Haubold, A.L. Rogach, A. Kornowski, M. Haase, H. Weller, A novel organometallic synthesis of highly luminescent CdTe nanocrystals, *J. Phys. Chem. B* 105 (12) (2001) 2260–2263.
 - [30] P. Dagtepe, V. Chikan, J. Jasinski, V.J. Leppert, Quantized growth of CdTe quantum dots; observation of magic-sized CdTe quantum dots, *J. Phys. Chem. C* 111 (41) (2007) 14977–14983.
 - [31] E.A. Lewis, R.C. Page, D.J. Binks, T.J. Pennycook, P. O'Brien, S.J. Haigh, Probing the core–shell–shell structure of CdSe/CdTe/CdS type II quantum dots for solar cell applications, *J. Phys.: Conf. Ser.* 522 (1) (2014) 012069.
 - [32] M. Califano, A. Franceschetti, A. Zunger, Lifetime and polarization of the radiative decay of excitons, biexcitons, and trions in CdSe nanocrystal quantum dots, *Phys. Rev. B* 75 (2007) 115401.
 - [33] D. Espinbarro-Velazquez, M.A. Leontiadou, R.C. Page, M. Califano, P. O'Brien, D.J. Binks, Effect of chloride passivation on recombination dynamics in CdTe colloidal quantum dots, *ChemPhysChem* 16 (6) (2015) 1239–1244.
 - [34] K. Nishikawa, Y. Takeda, T. Motohiro, D. Sato, J. Ota, N. Miyashita, Y. Okada, Extremely long carrier lifetime over 200 ns in GaAs wall-inserted type II InAs quantum dots, *Appl. Phys. Lett.* 100 (11) (2012) 113105.
 - [35] S. Tomić, Effect of Sb induced type II alignment on dynamical processes in InAs/GaAs/GaAsSb quantum dots: implication to solar cell design, *Appl. Phys. Lett.* 103 (7) (2013) 072112.
 - [36] S. Tomić, J. Miloszewski, E. Tyrrell, D. Binks, Design of core/shell colloidal quantum dots for meg solar cells, *IEEE J. Photovoltaics* 6 (1) (2016) 179–184, <http://dx.doi.org/10.1109/JPHOTOV.2015.2483368>.
 - [37] C.T. Smith, E.J. Tyrrell, M.A. Leontiadou, J. Miloszewski, T. Walsh, R.P.M. Cadirci, P. O'Brien, D. Binks, S. Tomić, Energy structure of CdSe/CdTe type II colloidal quantum dots—do phonon bottlenecks remain for thick shells? *Sol. Energy Mater. Sol. Cells* (2016), <http://dx.doi.org/10.1016/j.solmat.2015.12.015> submitted for publication.
 - [38] Z.-J. Jiang, D.F. Kelley, Role of surface states in the exciton dynamics in CdSe core and core/shell nanorods, *J. Phys. Chem. C* 114 (41) (2010) 17519–17528.
 - [39] R.C. Page, D. Espinbarro-Velazquez, M.A. Leontiadou, C. Smith, E.A. Lewis, S. J. Haigh, C. Li, H. Radtke, A. Pengpad, F. Bondino, E. Magnano, I. Pis, W. R. Flavell, P. O'Brien, D.J. Binks, Near-unity quantum yields from chloride treated CdTe colloidal quantum dots, *Small* 11 (13) (2015) 1548–1554.
 - [40] K. Gong, Y. Zeng, D.F. Kelley, Extinction coefficients, oscillator strengths, and radiative lifetimes of CdSe, CdTe and CdTe/CdSe nanocrystals, *J. Phys. Chem. C* 117 (39) (2013) 20268–20279.
 - [41] A. Javier, D. Magana, T. Jennings, G.F. Strouse, Nanosecond exciton recombination dynamics in colloidal CdSe quantum dots under ambient conditions, *Appl. Phys. Lett.* 83 (7) (2003) 1423–1425.
 - [42] Z.J. Jakubek, J. deVries, S. Lin, J. Ripmeester, K. Yu, Exciton recombination and unconverted photoluminescence in colloidal CdSe quantum dots, *J. Phys. Chem. C* 112 (22) (2008) 8153–8158.
 - [43] S.A. Crooker, T. Barrick, J.A. Hollingsworth, V.I. Klimov, Multiple temperature regimes of radiative decay in CdSe nanocrystal quantum dots: intrinsic limits to the dark-exciton lifetime, *Appl. Phys. Lett.* 82 (17) (2003) 2793–2795.
 - [44] M. Califano, Origins of photoluminescence decay kinetics in CdTe colloidal quantum dots, *ACS Nano* 9 (3) (2015) 2960–2967.
 - [45] C.-Y. Chen, C.-T. Cheng, C.-W. Lai, Y.-H. Hu, P.-T. Chou, Y.-H. Chou, H.-T. Chiu, Type-II CdSe/CdTe/ZnTe (core/shell/shell) quantum dots with cascade band edges: the separation of electron (at CdSe) and hole (at ZnTe) by the CdTe layer, *Small* 1 (2) (2005) 1215–1220.
 - [46] W. Shockley, H.J. Queisser, Detailed balance limit of efficiency of p–n junction solar cells, *J. Appl. Phys.* 32 (3) (1961) 510–519.
 - [47] M.C. Hanna, A.J. Nozik, Solar conversion efficiency of photovoltaic and photoelectrolysis cells with carrier multiplication absorbers, *J. Appl. Phys.* 100 (7) (2006) 074510.
 - [48] M.D. Archer, J.R. Bolton, Requirements for ideal performance of photochemical and photovoltaic solar energy converters, *J. Phys. Chem.* 94 (21) (1990) 8028–8036.
 - [49] (<http://redc.nrel.gov/solar/spectra/am1.5/>).
 - [50] D.J. Binks, Multiple exciton generation in nanocrystal quantum dots—controversy, current status and future prospects, *Phys. Chem. Chem. Phys.* 13 (2011) 12693–12704.
 - [51] M.C. Beard, A.G. Midgett, M. Law, O.E. Semonin, R.J. Ellingson, A.J. Nozik, Variations in the quantum efficiency of multiple exciton generation for a series of chemically treated PbSe nanocrystal films, *Nano Lett.* 9 (2) (2009) 836–845.
 - [52] M. Tagliazucchi, D.B. Tice, C.M. Sweeney, A.J. Morris-Cohen, E.A. Weiss, Ligand-controlled rates of photoinduced electron transfer in hybrid CdSe nanocrystal/poly(viologen) films, *ACS Nano* 5 (12) (2011) 9907–9917.
 - [53] A.J. Morris-Cohen, M.T. Frederick, L.C. Cass, E.A. Weiss, Simultaneous determination of the adsorption constant and the photoinduced electron transfer rate for a CdS quantum dot–viologen complex, *J. Am. Chem. Soc.* 133 (26) (2011) 10146–10154.
 - [54] J. Tang, K.W. Kemp, S. Hoogland, K.S. Jeong, H. Liu, L. Levina, M. Furukawa, X. Wang, R. Debnath, D. Cha, K.W. Chou, A. Fischer, A. Amassian, J.B. Asbury, E. H. Sargent, Colloidal-quantum-dot photovoltaics using atomic-ligand passivation, *Nat. Mater.* 10 (10) (2011) 765–771.
 - [55] A.B. Greytak, P.M. Allen, W. Liu, J. Zhao, E.R. Young, Z. Popovic, B.J. Walker, D. G. Nocera, M.G. Bawendi, Alternating layer addition approach to CdSe/CdS core/shell quantum dots with near-unity quantum yield and high on-time fractions, *Chem. Sci.* 3 (2012) 2028–2034.
 - [56] S. ten Cate, C.S.S. Sandeep, Y. Liu, M. Law, S. Kinger, A.J. Houtepen, J.M. Schins, L. D.A. Siebbeles, Generating free charges by carrier multiplication in quantum dots for highly efficient photovoltaics, *Accounts Chem. Res.* 48 (2) (2015) 174–181.
 - [57] G. Itskos, A. Othnos, T. Rauch, S.F. Tedde, O. Hayden, M.V. Kovalenko, W. Heiss, S.A. Choulis, Optical properties of organic semiconductor blends with near-infrared quantum-dot sensitizers for light harvesting applications, *Adv. Energy Mater.* 1 (5) (2011) 802–812.
 - [58] J.S. Kamal, A. Omari, K. Van Hoecke, Q. Zhao, A. Vantomme, F. Vanhaecke, R. K. Capek, Z. Hens, Size-dependent optical properties of zinc blende cadmium telluride quantum dots, *J. Phys. Chem. C* 116 (8) (2012) 5049–5054.